Surface Science 605 (2011) 528–538

Contents lists available at ScienceDirect

Surface Science

journal homepage: www.elsevier.com/ locate/susc

Spherical solid model system: Exact evaluation of the van der Waals interaction between a microscopic or submacroscopic spherical solid and a deformable fluid interface

Y.Z. Wang, B. Wang, X.M. Xiong, J.X. Zhang *

State Key Laboratory of Optoelectronic Materials and Technologies, and School of Physics and Engineering, Sun Yat-sen University, Guangzhou, 510275, China

ARTICLE INFO

Article history:
Received 14 September 2010
Accepted 9 December 2010
Available online 17 December 2010

Keywords:
vdW interaction
Derjaguin approximation
A microscopic or submacroscopic spherical solid
A deformable fluid interface

ABSTRACT

In many previous research work associated with studying the deformation of the fluid interface interacting with a solid, the theoretical calculation of the surface energy density on the deformed fluid interface (or its interaction surface pressure) is often approximately obtained by using the expression for the interaction energy per unit area (or pressure) between two parallel macroscopic plates, e.g. $\sigma(D) = -A/12\pi D^2$ *or* $\pi(D) = -A/6\pi D^3$ *for the van der Waals (vdW) interaction*, through invoking the Derjaguin approximation (DA). This approximation however would result in over- or even inaccurate-prediction of the interaction force and the corresponding deformation of the fluid interface due to the invalidation of Derjaguin approximation in cases of microscopic or submacroscopic solids. To circumvent the above limitations existing in the previous DA-based theoretical work, a more accurate and quantitative theoretical model, available for exactly calculating the vdW-induced deformation of a planar fluid interface interacting with a sphere, and the interaction forces taking into account its change, is presented in this paper. The validity and advantage of the new mathematical and physical technique is rigorously verified by comparison with the numerical results on basis of the previous Paraboloid solid (PS) model and the Hamaker's sphere-flat expression (viz. $F = -2Aa^3/(3D^2(D+2a)^2)$), as well as its well-known DA-based general form of $F/a = -A/6z_{p0}^2$.

1. Introduction

The interaction of fluid entities with each other or with solid bodies in the controlled gaseous or liquid environments is of fundamental importance in many technological and industrial processes, such as the froth flotation, drug delivery, protein and cell separation and so on. [1–5] Various techniques, including the surface force apparatus (SFA) [6,7], the so-called MASIF [8,9], the atomic force microscopy (AFM) [10,11] and the colloid probe atomic force microscopy (CP-AFM) etc. [2,8,9,12,13], were employed to detect these interaction forces involving the deformed fluid interfaces. However, knowledge of these interactions involving fluid interfaces (particularly in cases of microscopic or submacroscopic solids) and the resulted deformation of the fluid interface remain limited as yet, despite of great efforts and corresponding significant progresses in the experimental aspects made by scientists in recent years [4–6,14–16]. This is not only due to the complex underlying mechanism of surface forces, but also due to the deformation of the fluid interface that makes evaluating the corresponding interaction energy and quantifying the surface forces difficult [2–5,8–23].

Recently a physical question of what happens at and to the air-water interface as a solid is lowered toward the interface has attracted the scientists' interest. Cortat and Miklavcic [24–26] first performed a theoretical study by modeling the solid as a paraboloid shaped object to investigate this practical and fundamental problem. On the basis of this paraboloid solid (PS) model [23–25], the variations in the total surface force on the solid and its induced deformation of the air-water interface as a function of position of the paraboloid, paraboloid geometry, and strength of the attractive vdW force have been discussed, and the stability of the air-water interface subjected to the attractive vdW force had been extensively studied. Following up Cortat and Miklavcic's pioneering works [24–26], our group later investigated the universal and scaling law at the proximity of the paraboloid solid to the deformable air-water interface both in theory and experiments using AFM [27,28].

Without doubt the previous PS model has achieved the great success in the cases of macroscopic solids, nevertheless it seems unavailable in the cases of microscopic or submacroscopic solids, since how to exactly compute the vdW interaction energy between a deformed fluid interface and the paraboloid shaped solid is still ambiguous for the PS model [22,24–40]. To calculate the surface energy density of the fluid interface induced by the attractive vdW interaction of the paraboloid solid, through invoking the Derjaguin approximation [4–6] all of the corresponding previous theoretical

* Corresponding author.
E-mail address: stszjx@mail.sysu.edu.cn (J.X. Zhang).

0039-6028/$ – see front matter © 2011 Elsevier B.V. All rights reserved.
doi:10.1016/j.susc.2010.12.012

works [22,24–40] often employed an approximate closed form expression, which was derived analytically through a straightforward pairwise integration of interatomic potentials over a unit area of one surface and an infinite area of another surface (as shown in Fig. 1a) and given by [3,5,24–28],

$$\sigma(D) = -A/\left(12\pi D^2\right) \text{or} \sigma(D) = -A/\left(2D^2\right) \quad (1)$$

The whole interfacial vdW energy was then evaluated by integrating $\sigma(D)$ over the fluid interface, that is [26] $U_{vdW} = \iint_{\Lambda} \sigma dS = \int_0^{\infty} \sigma W(r) 2\pi r dr$, where Λ denotes the deformed fluid interface, and dS denotes the infinitesimal element of the interface.

From a theoretical and mathematical standpoint, the involved mathematical technique of using Eq. (1) to calculate $\sigma(D)$ and U_{vdW} was apparently based on the indistinct base assumption of the Derjaguin approximation [4–6,25,27] that *the characteristic size of the paraboloid shaped solid should be much larger compared to the separation D*, for which the effects of solid curvature are minimal and the Derjaguin approximation can apply. However, the previous numerical results based on the PS model, e.g. Eqs. (11) and (12) in Ref [24] and data of Table 2 in Ref [25], indicate that the characteristic size of an approaching microscopic or submacroscopic paraboloid shaped solid with the paraboloid splay parameter of $\lambda = 100 \sim 10{,}000\ \text{m}^{-1}$ is comparable to (or might be smaller than) its limiting separation from the interacting greatest-bulging fluid interface. This means that the above-mentioned base assumption evidently violates when calculating the vdW interaction involved in the microscopic (or submacroscopic) paraboloid shaped solid in the previous PS model [40,41]. This would thus result in the gross overestimations of the interfacial vdW interaction density of the fluid interface and the corresponding total vdW interaction energy in cases of the microscopic or submacroscopic paraboloid shaped solids, and further lead to misleading and anomalous theoretical predictions of the deformation of the air-water interface. [24–28,38,39]

The aim of this paper is to present an accurate and rigorous theoretical model system to exactly quantify the non-contact mesoscopic vdW interaction between an infinite planar fluid interface and a spherical solid, and the corresponding deformation of the fluid interface. This presented theoretical model circumvents the above-mentioned limitations of the PS model, and may be available for specialized applications in the factual CP-AFM (or common AFM) experiments quantifying the mesoscopic interaction between microscopic or submacroscopic solids and various fluid interfaces. Toward this, (in Section 2) we derive an analytical expression available for exactly calculating the vdW surface energy density of the fluid interface induced by an approaching solid, through modeling the interacting solid as a spherical particle and using Israelachvili's pairwise integration method [3] or the Hamaker approach [40,42]. Then, (in Section 3) an improved physical and mathematical model system of a deformable fluid interface interacting with a spherical particle (namely the spherical solid (SS) model, as shown in Fig. 2) is presented. Following, (in Section 4) this SS model system is employed to further investigate some interesting and ambiguous problems existing in this field, including the existence of stable and unstable profiles [25,27] in the SS model system, the roles of the vdW surface pressure distribution [3–6,43,44] across the fluid interface in the vdW-induced deformation of the fluid interface, the force-vs-separation (or the maximum deformation versus the separation) behaviors involved in the deformed fluid interface and their corresponding universal and scaling descriptions [27], as well as the limiting height at which a solid can approach the fluid interface [24]. Through successfully addressing these above practical and fundamental problems, and comparing with the corresponding numerical results obtained by the previous PS model and the predictions by the Hamaker's sphere-flat expression [42–44] ($F = -2Aa^3/(3D^2(D+2a)^2)$) and its DA-Based form of $F/a = -A/6z_{p0}^2$, the validity and accuracy of this new mathematical and physical technique is rigorously verified. Finally, summary and final remarks appear in Section 5.

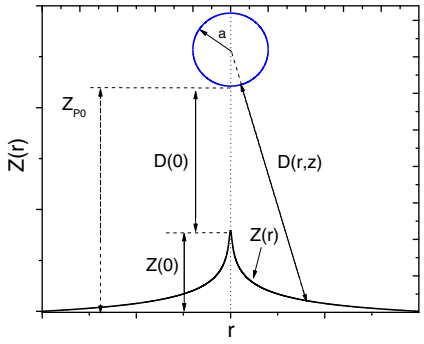

Fig. 2. A schematic of the spherical particle-fluid interface system in cross-section. $D(r,z)+a$ is the distance between the point on the deformable fluid profile $\{r,z(r)\}$ and the center of the spherical particle. z_{p0} denotes the lowest-most point of the spherical particle.

2. Interaction potentials between a sphere and a planar surface of unit area

2.1. Interaction between a molecule and a sphere

In a similar manner of Israelachvili's pairwise integration method [3] (or the Hamaker approach [42], see Fig. 1a) to deduce Eq. (1) (i.e.

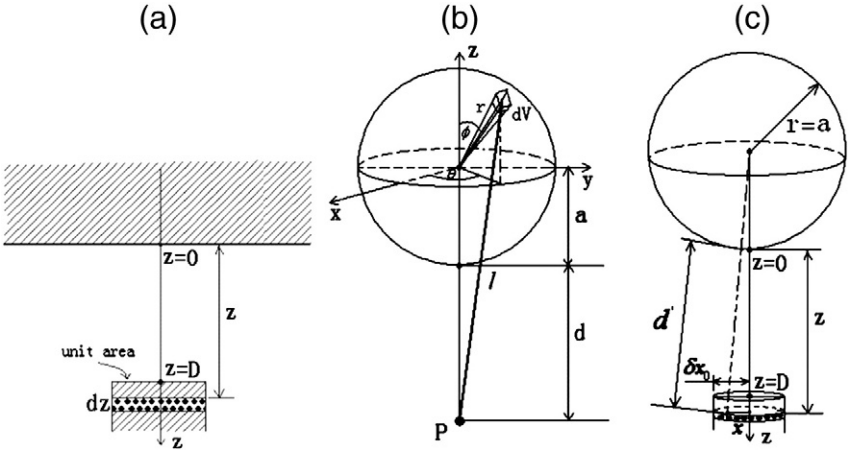

Fig. 1. Methods of integrating the interaction energies of molecules in condensed phases to obtain the interaction energies between two bodies: (a) a planar surface of unit area near an infinite planar surface [3]; (b) molecule near a spherical particle; (c) a circular planar surface of unit area near a spherical particle.

$\sigma(D) = -A/(12\pi D^2)$), we first investigate the interaction between a molecule (P) and a sphere of volume V, as shown in Fig. 1b. As the previous treatment [3], the pair potential between two atoms or small molecules is assumed to be purely attractive and of the form, $w(l) = -C/l^n$. With the assumption of additivity, the net interaction energy of a molecule and the spherical solid made up of like molecules will be the sum of its interactions with all the molecules in the body. From the elementary geometry in Fig. 1b, the number of molecules in the unit volume $dV = r^2 \sin\phi d\phi d\theta dr$ in the spherical coordinate system will be $\rho_1 r^2 \sin\phi d\phi d\theta dr$, where ρ_1 is the number density of molecules in the sphere. The distance (l) between this unit volume dV and the molecule (P) satisfies

$$l = \sqrt{(a+d)^2 + r^2 + 2r(a+d)\cos\phi}. \tag{2}$$

The net interaction energy for the molecule (P) at a distance d away from the sphere of radius a will therefore be

$$\begin{aligned} I(d;a) &= \int_V \rho_1 w(l) dV = -2\pi C\rho_1 \int_0^a r^2 dr \int_0^\pi \frac{\sin\phi}{l^n} d\phi \\ &= \frac{-2\pi C\rho_1}{(n-2)(a+d)} \int_0^a r dr \left[\frac{1}{(a+d-r)^{n-2}} - \frac{1}{(a+d+r)^{n-2}} \right] \\ &= \frac{-2\pi C\rho_1}{(n-2)(n-3)} \left[\frac{1}{d^{n-3}} + \frac{1}{(2a+d)^{n-3}} \right. \\ &\quad \left. + \frac{n-3}{(n-4)} \frac{1}{(a+d)(2a+d)^{n-4}} - \frac{n-3}{(n-4)} \frac{1}{(a+d)d^{n-4}} \right] \end{aligned} \tag{3}$$

for, $n \geq 4$

which for $n = 6$ (vdW forces [3]) becomes

$$I(d;a) = \frac{-\pi C\rho_1}{6} \left[\frac{1}{d^3} - \frac{1}{(2a+d)^3} + \frac{3/2}{(a+d)(2a+d)^2} - \frac{3/2}{(a+d)d^2} \right]. \tag{4}$$

Fig. 3 exactly shows the relation between $I(d;a)$ and d/a. It can be seen that the smaller the distance (d) is (or the larger the sphere radius (a) is), the larger the vdW interaction energy between a molecule and a spherical solid is. From Eq. (4) and Fig. 3 we can further see that if $a \gg d$ or if $a/d \to \infty$, indicating the sphere is much larger comparing to the separation, Eq. (4) can be simplified to be

$$I(d;a) \approx -\pi C\rho_1 / 6d^3, \tag{5}$$

which had been obtained by Israelachvili [3] to describe the vdW interaction between a molecular and a infinite planar solid surface.

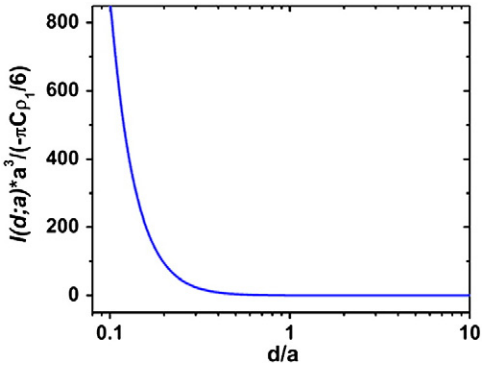

Fig. 3. Plot of $I(d;a) \times a^3/-\pi C\rho_1/6$ versus d/a by using Eq. (4).

2.2. Interactions between a sphere and a planar surface of unit area

We then calculate the interaction energy between a spherical solid and a circular planar surface, as shown in Fig. 1c. Likewise, we start with a thin circular sheet of molecules of area $\pi\delta x_0^2$ and thickness dz at a distance z away from the lowest-point of the sphere. From the elementary geometry in Fig. 1c and Eq. (3), and with the further assumption of additivity, the interaction energy between this sheet and the sphere is $\int_0^{\delta x_0} I(d';a)\rho_2 2\pi x dx dz$. in the cylindrical coordinate system, where ρ_2 is the number density of molecules in the circular cylinder and $d' = \sqrt{(z+a)^2 + x^2} - a$. Thus, for the sphere and the circular planar surface of unit area, we approximately have

$$\sigma_{unit}(D;a) = \int_D^\infty \rho_2 \frac{1}{\pi\delta x_0^2} \int_0^{\delta x_0} I(d';a) 2\pi x dx dz, \tag{6}$$

which can furthermore be rewritten to be

$$\sigma_{unit}(D;a) = \int_D^\infty \rho_2 H(z;a;\delta x_0) dz, \tag{7}$$

through defining a function such that

$$H(z;a;\delta x_0) := \frac{2}{\delta x_0^2} \int_0^{\delta x_0} I(d';a) x dx \tag{8}$$

It is important to note that Eq. (6) or Eq. (7) exactly characterizes the average quantity of the surface interaction energy density on the circular planar surface of area $\pi\delta x_0^2$. But the corresponding analytical form of Eq. (6) or Eq. (7) seems unavailable due to their too complicated mathematical integration. Nevertheless, this does not prevent us from deducing an analytical expression for exactly describing the vdW interaction energy between the sphere and a planar surface of unit area, which is denoted by σ in the following discussion.

From the above discussions in Section 1 we note that determination of U_{vdW} induced by the approaching solid is often accomplished by integrating σ over the deformed fluid interface, i.e. $U_{vdW} = \iint_A \sigma dS$. From a mathematical integral standpoint, σ is obviously signified to be the limit of σ_{unit} (described by Eq. (6) or (7) for $n = 6$) as the area of the upper circular base of the circular cylinder approaches infinitesimal (i.e. $\pi\delta x_0^2 \to 0$, see Fig. 1c). Hence, from Eq. (6)–(8) we can obtain

$$\begin{aligned} \sigma &= \lim_{\pi\delta x_0^2 \to 0} \sigma_{unit}(D;a) = \lim_{\delta x_0 \to 0} \int_D^\infty \rho_2 H(z;a;\delta x_0) dz \\ &= \int_D^\infty \rho_2 \left[\lim_{\delta x_0 \to 0} H(z;a;\delta x_0) \right] dz, \end{aligned} \tag{9}$$

where

$$\lim_{\delta x_0 \to 0} H(z;a;\delta x_0) = \lim_{\delta x_0 \to 0} \frac{2}{\delta x_0^2} \int_0^{\delta x_0} I(d';a) x dx. \tag{10}$$

Since $d' = \sqrt{(z+a)^2 + x^2} - a$ (see Fig. 1c), for all x in $[0, \delta x_0]$, $d'(x) \geq d'(x=0)$, from Fig. 3 or Eq. (4) it is easy to see that it satisfies $|I(d'(x);a)| \leq |I(d'(x=0);a)|$ and the approximation can be made by $I(d'(x);a) \approx I(d'(x=0);a)$ as δx_0 is much less and approaches infinitesimal. Eq. (10) can thus be simplified to be,

$$\lim_{\delta x_0 \to 0} H(z;a;\delta x_0) \approx \frac{2I(d'(x=0);a)}{\delta x_0^2} \int_0^{\delta x_0} x dx \approx I(d'(x=0;a) \tag{11}$$

in which $d'(x=0;a) = \left(\sqrt{(z+a)^2 + x^2} - a \right)|_{x=0} = z$. From Eqs. (9) and (11) we then obtain $\sigma(D;a) = \int_D^\infty I(z;a)\rho_2 dz$. Finally,

substituting Eq. (4) into this equation and integrating over z from D to ∞ produces

$$\sigma(D;a) = -\frac{A}{12\pi}\left[\frac{1}{D^2} - \frac{1}{(2a+D)^2} - \frac{3}{a^2}\left(\ln\frac{D}{D+2a} - \frac{a}{D+2a} - \frac{a}{D}\right)\right], \tag{12}$$

where $A=\pi^2 C\rho_1\rho_2$ is the conventional Hamaker constant [3]. It is clear that Eq. (12) is a more efficient analytical expression for exactly calculating the vdW surface energy density without any restrictions of the size of the sphere and the separation [3–5,39,43,44]. If assuming $D \ll a$, Eq. (12) can transform into Eq. (1) (i.e. $\sigma(D) \approx -A/(12\pi D^2)$). The assumption $D \ll a$ is clearly the same as our above-mentioned base assumption of the Derjaguin approximation [3–5,39]. This thus tells us that if in cases of the closer separation or large size of the sphere, the vdW surface energy density can be approximately calculated by using Eq. (1) through invoking $D \ll a$, as used in the previous researches.

Fig. 4 shows the comparison of the vdW surface energy densities respectively calculated by using Eqs. (1) and (12). The data curves describe the variations of the dimensionless vdW interaction energy $(-\sigma/A)$ with the surface-to-surface separation distance between the spherical solid and the unit area plane surface (D, see Fig. 4a), as well as with the sphere radius (a, see Fig. 4b). It is clear that Eq. (12) predicts the vdW surface energy density smaller than Eq. (1), and that this discrepancy becomes more distinct as the base assumption $D \ll a$ is gradually violated due to increasing the separation distance or decreasing the radius of the sphere. As $D > a/28$, the relative deviation, which is defined to be $(\sigma_{Eq.1} - \sigma_{Eq.12})/\sigma_{Eq.12}$, is evidently much larger than 10%. Such result is quite analogous to the one reported by Bhattacharjee and Elimelech [39], involved in the comparison of the vdW interaction energies between a sphere and an infinite flat plate obtained using the surface element integration (SEI) technique and the DA one. From Bhattacharjee and Elimelech's previous study [39], we can know that the use of Eq. (1) to calculate the vdW surface energy density induced by a sphere is analogous to be a DA technique; the obvious discrepancy when $a<28D$ as shown in Fig. 4 factually results from the gross overestimation of the vdW interaction energy density calculated by Eq. (1) due to the violation of the base assumption ($D \ll a$) in cases of the small sphere (or the large separation); and that a remarkable improvement can be obtained by using Eq. (12) through ruling out the limitation of the assumption $D \ll a$.

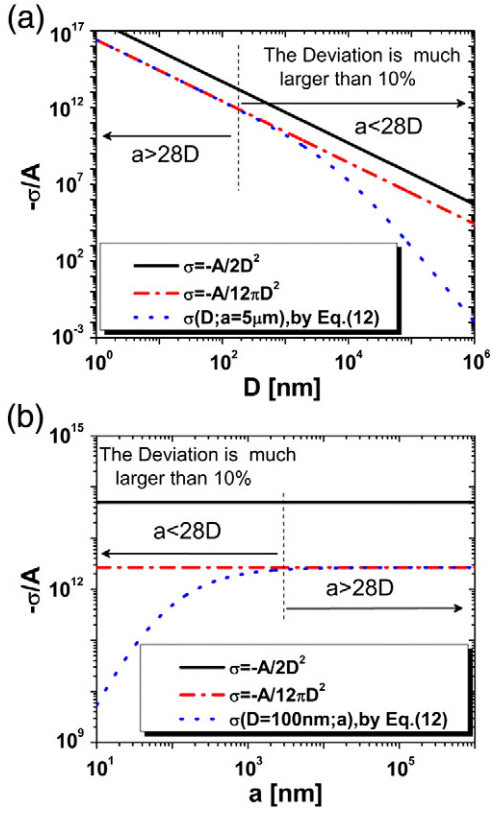

Fig. 4. Comparison of the variations of the scaled attractive vdW interaction $(-\sigma/A)$ between a spherical solid and a plane surface of unit area with (a) the separation distance and (b) the size of the spherical particle obtained respectively from Eqs. (1) and (12). The thin dashed line characterizes the boundary situation of $a \approx 28D$, at which the deviation (which is defined to be $(\sigma_{Eq.1} - \sigma_{Eq.12})/\sigma_{Eq.12}$) is large up to about 10%. Thereinto, $\sigma_{Eq.1}$ denotes the result calculated by $\sigma(D) = -A/(12\pi D^2)$, and $\sigma_{Eq.12}$ denotes the one by Eq. (12).

Consequently it can be conclude that Eq. (12) is a straightforward approach, similar to the SEI technique [30,39] but having an analytical form, to provide a possibility to exactly calculate the vdW surface energy density in the deformed fluid interface induced by not only a interacting macroscopic spherical solid but also the microscopic or submacroscopic one. Moreover emphasis should be placed that Eq. (12) is different from Hamaker's results [39,42], which characterizes the vdW interaction energy between a sphere and an infinite surface, despite the last complex term in Eq. (12) being quite similar to Hamaker's results [39,42], and the first and second terms in Eq. (12) seemingly decay faster than other terms.[1]

3. The spherical solid (SS) model system

In this section we would introduce the improved mathematical and physical model system based on Eq. (12), as shown in Fig. 2, for numerically investigating the attractive nonretarted vdW-induced deformation of a fluid interface interacting with an approaching solid. This theoretical model considers the approaching solid having a simplest configuration of a sphere with the radius of a, and has the major advantage that the exact calculation of the total vdW interaction energy taking into account the changes of the deformed fluid interface is available without the restriction of the above-mentioned base assumption of the Derjaguin approximation. Accordingly, as in the previous studies [18,24–27,35,36], in the calculations of the equilibrium configuration of the liquid surface interacting with a spherical particle, the balance of three forces is considered:

(1) the surface tension of the fluid interface;
(2) the van der Waals attraction between the spherical particle and the fluid interface;
(3) the gravitational force acting to oppose the deformation of the fluid interface.

In cylindrical coordinates the total energy of the deformed fluid interface $\{r,z(r)\}$ that accounts for the above three contributions can be written as [27]

$$U = 2\pi\int_0^\infty r\left[(\gamma+\sigma)W(r) + \frac{G}{2}z^2\right]dr, \tag{13}$$

where $W(r) = \sqrt{1+z_r^2}$ is an area scaling factor, $G=\Delta\rho g$ is the notation by multiplying the density difference $\Delta\rho$ with the gravitational acceleration g, γ is the surface tension of the fluid interface, and σ (depicted by Eq. (12)) characterizes the vdW interaction energy between the spherical particle and a planar surface of unit

[1] The calculated results by Eq. (12) shown in Fig. 4 clearly show that with varying the D/a value, the first term in Eq. (12) is large than the second term and the third complex one, despite the first and second term, having the square term, seemingly decay faster than each term in the third complex.

area at $(r, z(r))$ separated by a distance $D(r,z)$. From Fig. 2, $D(r,z)$ satisfies

$$D(r,z) = \sqrt{(z_{P0} + a - z)^2 + r^2} - a. \tag{14}$$

In terms of the fundamental theorem [4,5,27] that an equilibrium surface profile of the fluid interface $\{r,z(r)\}$ can be achieved when the total free energy of the fluid interface is minimum or maximum, an Euler–Lagrange (E–L) differential equation can then be obtained [27]

$$\frac{d}{dr}\left[\frac{rz_r(r)}{W}(\gamma + \sigma(r,z))\right] = r\left[Gz + W\frac{\partial\sigma(r,z)}{\partial z}\right]. \tag{15}$$

The free fluid surface profile can thus be determined self-consistently by numerically solving the above E–L differential equation with two optimally refined boundary conditions $\{z_r(0) = 0, z(\infty) = 0\}$ through using the collocation–integration technique [24–28].

After determination of the fluid interface profile $\{r,z(r)\}$, the vdW surface energy density on the interface can be calculated by using Eqs. (12) and (14), and the corresponding imposed vdW surface pressure distribution across the deformed fluid interface can also be obtained by [3–6,23,33,36,37]

$$P_z(r,z) = \frac{\partial\sigma}{\partial z} = \frac{\partial\sigma}{\partial D}\frac{\partial D}{\partial z} = -\Pi(D)\frac{\partial D}{\partial z}, \tag{16a}$$

and

$$P_r(r,z) = \frac{\partial\sigma}{\partial r} = \frac{\partial\sigma}{\partial D}\frac{\partial D}{\partial r} = -\Pi(D)\frac{\partial D}{\partial r}, \tag{16b}$$

where $\Pi(D)$ is the vdW-induced disjoining pressure acting in the direction of the normal to the interface at $(r, z(r))$ separated by a distance $D(r,z)$, and $P_z(r,z)$ and $P_r(r,z)$ respectively represent the components of this vdW surface pressures acting in the z-direction and in the horizontal (or lateral) direction [23,33,36,37]. It is clearly indicative from Eqs. (16a) and (16b) that the $P_z(r,z)$ and $P_r(r,z)$ pressures are respectively responsible for the longitudinal and lateral deformation of the fluid interface. Since the vdW force on the fluid profile is equal and opposite to the one exerted on the spherical solid, the vertical component (z axis) of the force acting on the spherical solid can thus be obtained by integrating the corresponding z-direction pressure distribution, $P_z(r,z)$, over the deformed fluid interface, i.e. [23–27,33,36,37]

$$F = \int_0^\infty P_z(r,z)W(z_r)2\pi r dr. \tag{17}$$

From the above analysis, it is clear that with simply replacing the paraboloid shaped solid by the spherical one, and calculating the vdW surface energy density by using Eq. (12) instead of Eq. (1), the improved SS theoretical model enables the calculation of the vdW surface energy involving the deformed fluid interface to be exact and thus conquers the above-mentioned disadvantages of the previous PS model system [25,27]. This thus present a possibility to exactly investigate the interaction involved in the deformed fluid interface and the resulted deformation of the fluid interface for cases of the approaching microscopic or submacroscopic solids.

4. Numerical results and discussion

4.1. Stable and unstable solutions to the E–L equation based on the SS theoretical model

It was known [24,25] that in the previous PS model there exists two legitimate solutions to the E–L equation near the mathematical existence limit [27,29–39], one represents a stable (local minimum energy) solution, and the other represents the unstable (local maximum energy) solution. From the mathematical point, in the SS theoretical model system, the calculation of the vdW surface energy density (viz. σ) in the E–L differential equation (viz. Eq. (15)) by using Eq. (12) instead of Eq. (1) would result in a distinct discrepancy of the calculated energy functional, in particular for cases when the Derjaguin approximation invalidates. Our first task here is to check the existence of these two possible stable and unstable solutions to Eq. (15) based on the SS theoretical model.

We show both stable and unstable profiles obtained by solving Eq. (15) for a sequence of spherical particle heights (z_{p0}) in Fig. 5. It is clear that the stable profiles show increasing deformation as the sphere is lowered, contrarily the unstable ones show the opposite tendency of diminishing their degree of deformation; and that the sequences curves converge in both figures to the limiting profile found at the critical solid height of $z_{p0} \approx 56.0$ *nm*. The overall behavior in Fig. 5 quite coincides with the one [25,27] previously predicted on the basis of the PS model, despite the corresponding profile deformation obtained by the PS model seeming much larger due to the gross overestimation of the total vdW interaction energy and the corresponding existence limit might also be modified [25,27–30]. This coincidence thus presents a straightforward evidence on the validity of numerical results on the basis of the SS theoretical model, and also further confirms the rationality of the existence of the unstable fluid interface previously predicted in the PS model.

For details of the nature of the two above solutions and their states of stability see the previous refs [24–27]. In this paper we focus attention only on the stable solution, and to further check and ensure the validity and advantage of the SS theoretical model to address the practical problems, which are usually unavailable or poor predicted by the previous PS model, or remain ambiguous as yet.

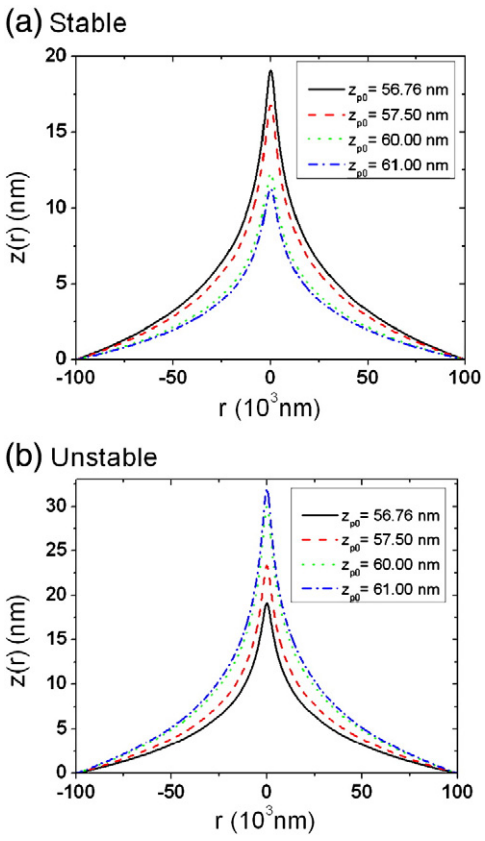

Fig. 5. Stable (a) and unstable (b) solutions of Eq. (15) involved in using Eq. (12) to calculate the vdW surface energy density (σ), and their behaviors as a function of the spherical particle heights. The physical parameters are $a = 100\,\mu m$, $A = 2.0*10^{-19}$ J, $\gamma = 72$mN/m and $\Delta\rho = 996.910$ kg/m^3.

4.2. The vdW surface pressure distribution across the deformed profile dependent on system parameters

Previous studies [3–6,12–16,18–21,29–39] have suggested that the deformation of the fluid interface interacting with a solid is controlled by both the surface pressure across the interface due to the imposed stress and the surface tension of this fluid interface. But, to our knowledge, the understanding of the corresponding vdW surface pressure distribution on the deformed fluid interface induced by the solid, as well as the effects of the surface tension, still remains limit, due to the unavailability of exact calculation of the vdW surface energy density [24–27]. Our main object in this section is to use the SS model to investigate the vdW surface pressure distributions across the deformed interface dependent on the system parameters, including the interacting sphere height (z_{p0}), the vdW interaction strength (A), the radius of this interacting sphere (a) and the surface tension of the fluid interface (γ).

From Figs. 8 and 9 we find that the $P_z(r,z)$ and $P_r(r,z)$ distributions vary regularly with varying the system parameters, better corresponding to the dependence of the deformation on the system parameters shown in Figs. 6 and 7. Thereinto, Figs. 8a and 9a, for example, show that as decreasing the sphere height, the average $P_z(r,z)$ strength gradually increases and the corresponding "effective area" [3] becomes smaller, simultaneously the corresponding average $P_r(r,z)$ strength increases. This results in the increases of the longitudinal deformation and the lateral (or horizontal) extent of deformation, as obviously shown in Fig. 6a and the inset of Fig. 7a. Also, Figs. 6b, 7b, 8b and 9b (or Figs. 6c, 7c, 8c and 9c), demonstrates the effects of changing the vdW surface pressure distribution to the longitudinal and lateral deformation of the fluid interface by varying the Hamaker constant (or the sphere radius). Through using the special Gauss distribution formula [45] $f(x) = \frac{f_0}{\sqrt{2\pi}\eta} e^{-2x^2/\eta^2}$ to fit the histogram data of Fig. 8, at which η has the physical significance of characterizing the size of the "effective area" [3] of the vertical component of the vdW interaction, and $P_{max} \equiv f_0 / \sqrt{2\pi}\eta$ approximately measures the average strength of the vdW surface pressure on this effective area, we can then obtain the corresponding P_{max} and η data given in Table 1, to quantitatively and accurately support the above analysis.

In addition, Figs. 8d and 9d show that both the $P_z(r,z)$ and $P_r(r,z)$ distribution appears unchanged with varying the surface tension from 10mN/m to 150mN/m, despite of the prominent changes of the corresponding longitudinal and lateral deformation as shown in Figs. 6d and 7d. This obviously indicates that varying the surface tension in controlling the deformation of the fluid interface is independent of the vdW surface pressure distribution across the interface, in cases of weak vdW interaction and moderate deformation [29–31]. Whereas, if for cases of strong vdW interaction and great fluid deformation, the corresponding interaction and deformation behaviors would be more complex, due to the strong coupled effects from both the surface tension and the surface pressure distribution across the deformed interface.

From Table 1 and Figs. 6(a-d) to 9(a,-d) we thus can qualitatively conclude that, for cases of the fixed surface tension, the $P_z(r,z)$ and $P_r(r,z)$ distributions are respectively responsible for the longitudinal and lateral deformation of the fluid interface, the stronger the average $P_z(r,z)$ and $P_r(r,z)$ strengths are, the larger the longitudinal and lateral deformation of the fluid interface will be; and that for cases of weak interaction and moderate deformation, the role of the surface tension in controlling the deformation of the fluid interface is independent of the vdW surface pressure distribution across the interface, quite similar to the effective spring constant of the fluid interface.

4.3. Scaled dependences of Profile Peak and vdW force on height of the solid

We next are to use the SS model to investigate the dependences of the deformation peak ($z(0)$) and the corresponding interacting force (F) on the spherical particle position (z_{p0}) for various values of interaction strength and radius of the spherical particle of the μm order, which is of particular interest for applications in the AFM

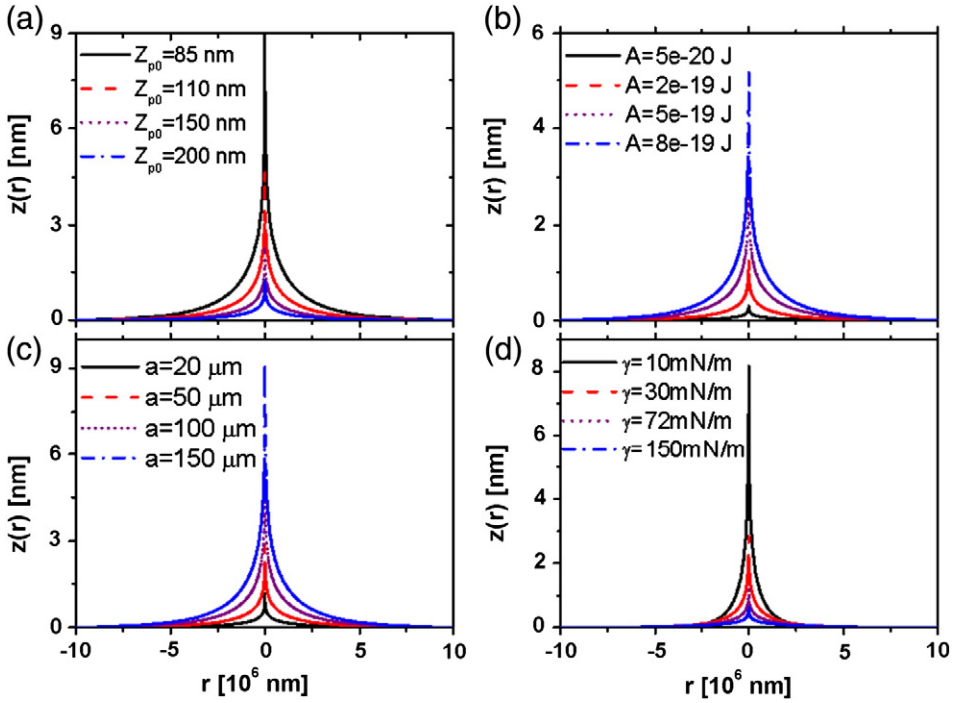

Fig. 6. Profiles for (a) different heights of the spherical particle, (b) different strengths of the vdW interaction, (c) different radius of the spherical particle, and (d) different values of tension surface. The physical parameters are a = 100 μm, $A = 2.0*10^{-19}$ J, $\gamma = 72$mN/m and $\Delta\rho = 996.910$ kg/m^3 for (a); $a = 100$ μm, $z_{p0} = 200$.nm, $\gamma = 72$mN/m and $\Delta\rho = 996.910$ kg/m^3 for (b); $A = 2.0*10^{-19}$ J, $z_{p0} = 200$.nm, $\gamma = 72$mN/m and $\Delta\rho = 996.910$ kg/m^3 for (c); $a = 100$ μm, $z_{p0} = 200$.nm, $A = 2.0*10^{-19}$ J, and $\Delta\rho = 996.910$ kg/m^3 for (d).

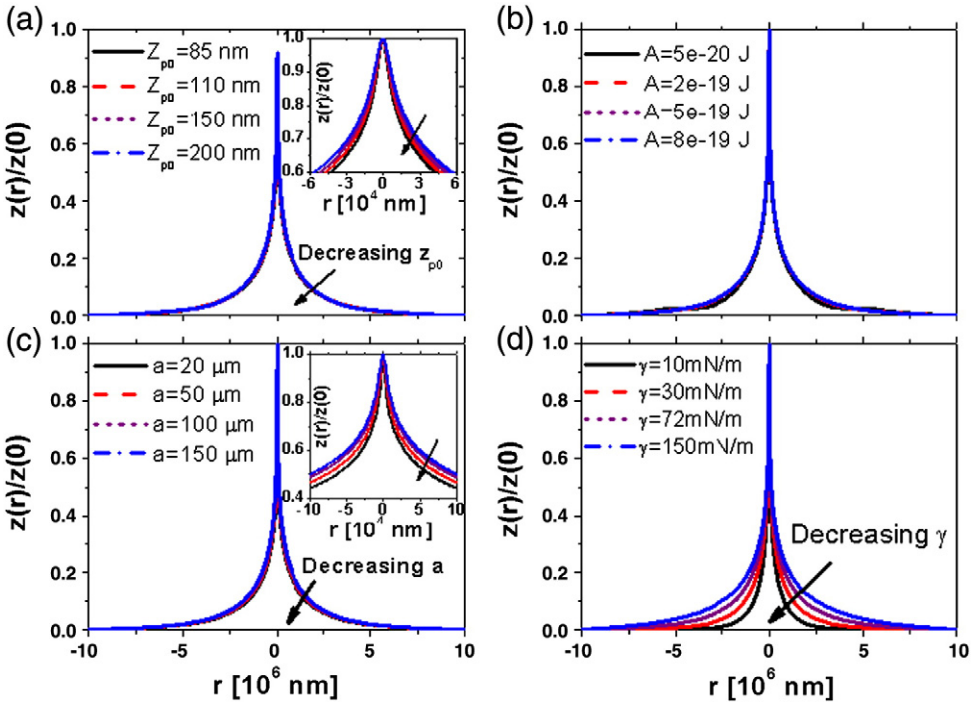

Fig. 7. Normalized profiles of the corresponding profiles shown in Fig. 6.

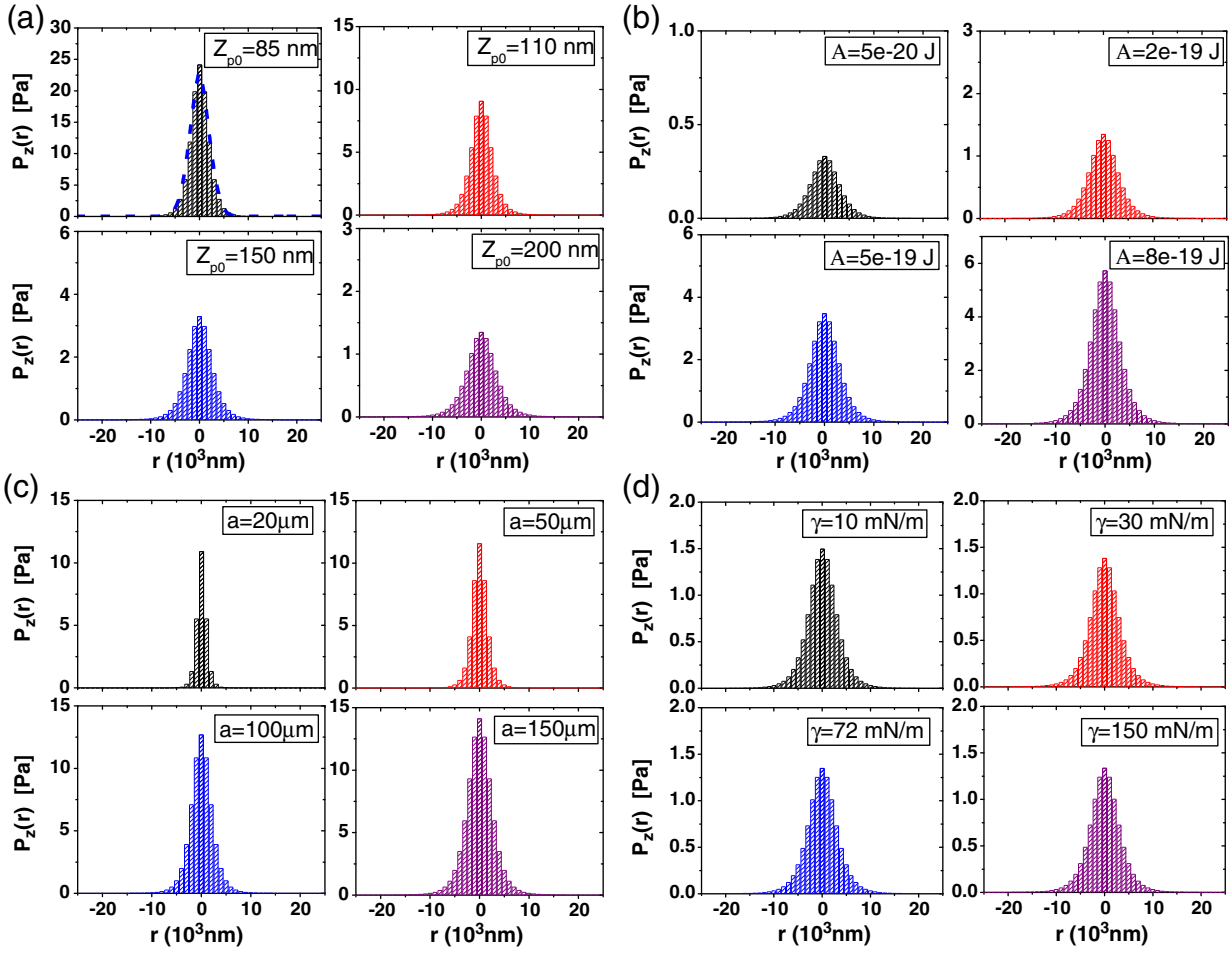

Fig. 8. vdW surface pressure (acting in the z-direction) distribution $P_z(r)$ on the deformable fluid interface interacting with a spherical solid for (a) different heights of the spherical particle, (b) different strengths of the vdW interaction, (c) different radius of the spherical particle, and (d) different values of tension surface. The $P_z(r)$ data is calculated by using Eqs. (12), (14) and (16a), as well as the deformed profile data $\{r,z(r)\}$ of Fig. 6. The physical parameters are the same as those taken in Fig. 6. The dashed curve in the up-left figure of Fig. 8.(a) (viz. $z_{p0}=85$ nm) is the result obtained by the Gaussian fitting.

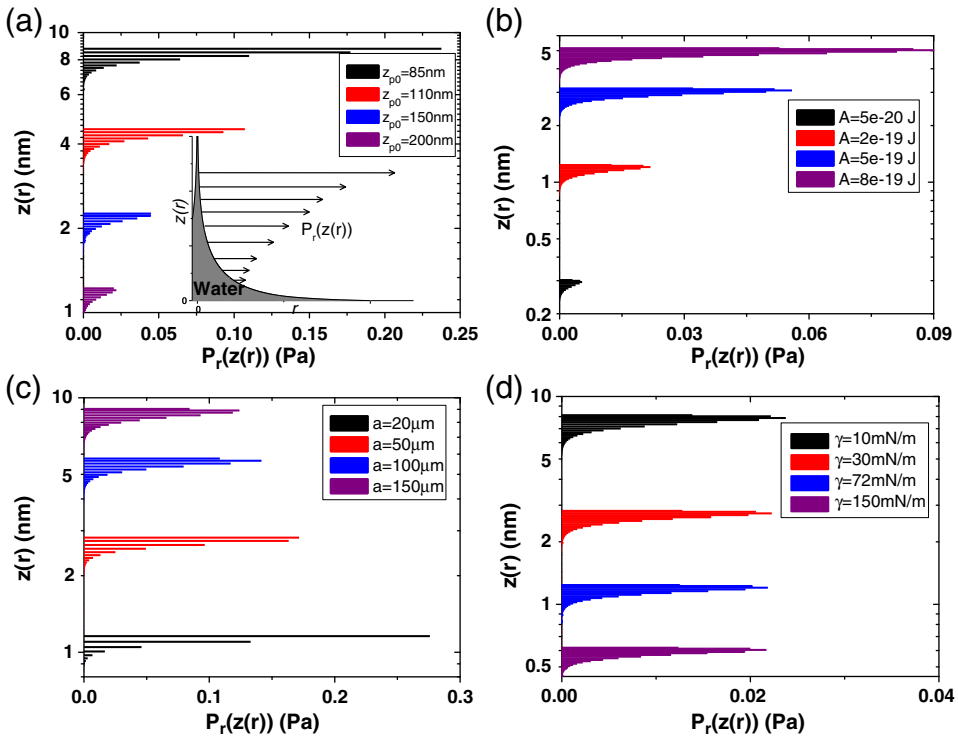

Fig. 9. The dependence of the corresponding horizontal-direction vdW surface pressure $P_r(z(r))$ distribution on the system parameters (z_{p0}, A, a and γ), plotted as the $z(r)\sim P_r(z(r))$ bar. The $P_r(z(r))$ data is calculated by using Eqs. (12), (14) and (16b), as well as the deformed profile data $\{r,z(r)\}$ of Fig. 6 (Note that the profile data $\{r,z(r)\}$ of $r>0$ is only concerned here). The physical parameters are the same as those taken in Fig. 6. The inset of Fig. 9a shows the cross-sectional schematic of the vdW surface pressure $P_r(z(r))$ distribution on the deformed fluid interface.

experiment (in particular the CP-AFM) [2–6,12,13,20–30] quantifying the mesoscopic interaction between microscopic or submacroscopic solids and the fluid surfaces.

Open symbol curves in both Figs.10 and 11 respectively illustrate the general qualitative and specific quantitative behaviors of the functions, $z(0;z_{p0})$ and $F(z_{p0})$, for various values of the radius of the approaching spherical solid ($a \in [1,1000]\mu m$) and the interaction strength ($A\in[2500]\times 10^{-21}$ J). Thereinto the leftmost extreme points of each of the curves are the sets of critical limiting points [24,25] ($[z_{p0,min}, z(0,z_{p0,min})]$ and $[z_{p0,min}, F(z_{p0,min})]$), determined in terms of the solvability limits of Eq. (15). These results are clearly in line with the general expectations: deformation and interacting force increase as the sphere is lowered toward the fluid interface with the extent of deformation and vdW force increasing with increasing A and a. Nevertheless, by comparing with the PS-model predictions in the range $\lambda\in[100,10,000]m^{-1}$ shown as solid symbol curves in Fig. 10 we see that obvious discrepancies appear, despite the range $\lambda\in[100,10,000]m^{-1}$ in the previous PS model system was claimed [24,25] to scale the microscopic or submacroscopic size of the paraboloid solid. Values of $z(0)$ and the vdW force (F) predicted by the previous PS model are clearly much larger than those predicted by the SS model, even the results for $\lambda = 10{,}000\ m^{-1}$ are also quite larger than the ones for $a = 1000$ μm. In light of the above discussion, these discrepancies mainly result from the gross overestimation of the vdW interaction due to the invalidation of the Derjaguin approximation in the PS model.

Furthermore, scaling both z_{p0} and F of each data set in Figs. 10b and 11b by corresponding critical values of $z_{p0,min}$ and $F(z_{p0,min})$ gives rise to the resultant normalized curves as shown in Fig. 12. In like manner as in the previous refs [27], through fitting we find that they also obey the scaling power law given by [27]

$$\tilde{F} = C_F\, \tilde{z}_{p0}^{-b_F}, \tag{18}$$

at which value of the coefficient b_F is approximate 2.0 and increases dramatically with decreasing z_{p0} nearby $z_{p0,min}$. This scaled behavior is clearly consistent with those reported in the previous refs [27] based on the PS model. The scaling parameter b_F is dependent on both the geometries of the solid and the fluid interface, and can be used to indicate the longitudinal deformation and instability of the whole fluid

Table 1
Values of fitting parameters of the Gauss distribution function[44], $f(x) = \frac{f_0}{\sqrt{2\pi}\eta} e^{-2x^2/\eta^2}$, used for fitting the $P_z(r)$ distribution data of Fig. 8.(a-d).

(a)			(b)			(c)			(d)		
Z_{p0} (nm)	P_{max} (Pa)	η (μm)	A (10^{-21} J)	P_{max} (Pa)	η (μm)	a (μm)	P_{max} (Pa)	η (μm)	γ (mN/m)	P_{max} (Pa)	η (μm)
85	23.69	3.57	50	10.84	5.81	20	0.33	1.79	10	1.48	5.68
110	9.00	4.22	200	11.45	5.79	50	1.34	2.86	30	1.40	5.77
150	3.27	4.99	500	12.69	5.76	100	3.49	3.97	72	1.35	5.79
200	1.33	5.79	800	14.15	5.73	150	5.71	4.72	150	1.35	5.80

Note that $P_{max}\equiv f_0/\sqrt{2\pi}\eta$ characterizes the maximal vdW surface pressure across the deformed fluid interface (i.e. $P_z(r=0)$); and η here has the physical significance of characterizing the size of the effective "interacting area"[3] induced by the vertical component vdW surface pressure on the fluid interface.

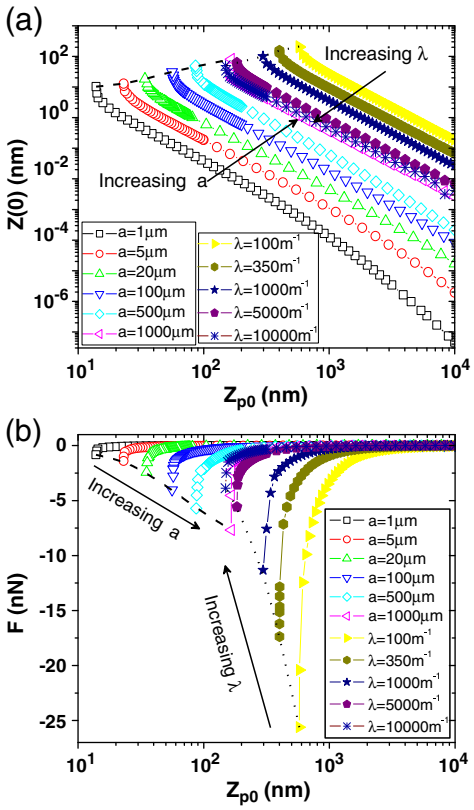

Fig. 10. Numerical calculations of the functions $z(0, z_{p0})$ (a) and $F(z_{p0})$ (b) with varying the size of the approaching solid based on the PS model (curves with solid symbols) and the SS model shown in Fig. 1 (curves with open symbols). The physical parameters are $\gamma = 72$mN/m, $A = 2.0\times10^{-19}$ J and $\Delta\rho = 996.910$ kg/m^3; and size constants $\lambda \in \{100,350,1000,5000,10,000\}$m^{-1} for the PS model, constants a$\in\{1,5,20,100,500,1000\}$μm for the SS model.

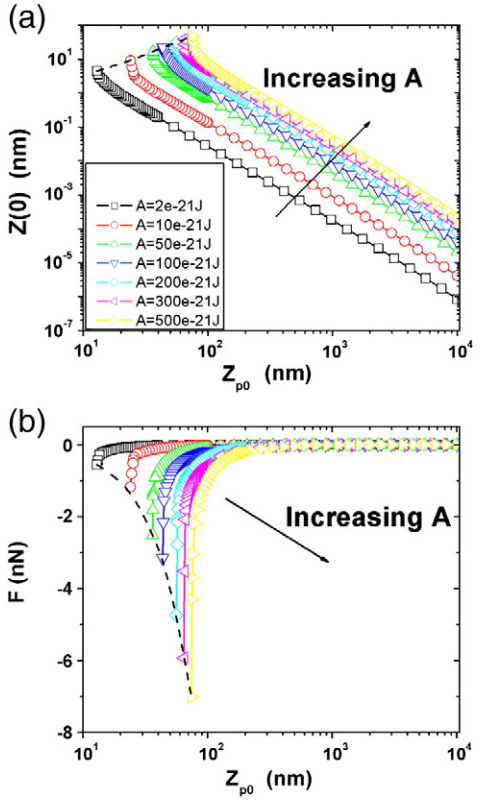

Fig. 11. Numerical calculations of the functions $z(0, z_{p0})$ (a) and $F(z_{p0})$ (b) with varying the interaction strength, A, based on the SS model. The physical parameters are $\gamma = 72$mN/m, $\Delta\rho = 996.910$ kg/m^3, a = 100 μm and Hamaker constants $A\in\{2,10,50,200,300,500\}\times10^{-21}$ J.

interface. The larger the value of b_F is, the larger the longitudinal deformation and the less stable the fluid interface will be. Nevertheless, when the sphere is far from the limiting position and the corresponding deformation of the air–water interface is very small, value of b_F decays gradually to 2.0 with increasing the sphere radius (as shown in inset of Fig. 12a), and satisfies $b_F \approx 2.01 + 1.08\,e^{-a^*/1.69} + 0.69e^{-a^*/8.77} + 0.11e^{-a^*/136.5}$, where $a^* = a/a_0$ and $a_0 = 1$ μm. Such behavior is clearly different and opposite to the dependence of other scaling parameter (b) on λ reported previously [27]. Various complicated factors lead to this difference. The main factors are that b_F indicates the longitudinal deformation for the whole profile whereas b is only for the apex of fluid interface; and that the results for large $\tilde{z}_{p0}$ shown in Fig. 12a and its inset equivalently describes the effects of varying the size of a sphere of the μm order to the vdW interaction between this sub-macroscopic solid sphere and an infinite less-deformed fluid interface that is far away, at which both the DA approximation and its base assumption invalidate.

It is known that the well-known DA-based sphere-flat expression [3–6,42,43] $F/a = -A/6z_{p0}^2$ is the simplified format of the Hamaker's sphere-flat one, $F = -2Aa^3/(3z_{p0}^2(z_{p0}+2a)^2)$, based on the assumption that $a \gg z_{p0}$ through invoking the Derjaguin approximation. To further validate the behavior in Fig. 12a and its above-mentioned interpretation, we compare the normalized vdW force ($-F$/a) versus z_{p0} behavior predicted by the SS model to the ones respectively by $F = -2Aa^3/(3z_{p0}^2(z_{p0}+2a)^2)$ and $F/a = -A/6z_{p0}^2$ with $A = 2\times10^{-19}$ J, as shown in Fig. 13. From Fig. 13 it can be seen that good agreement between the SS-model predictions and the $F = -2Aa^3/(3z_{p0}^2(z_{p0}+2a)^2)$ one is achieved in the cases of the smaller sphere far away from the fluid interface, whereas obvious deviations from the DA-based $F/a = -A/6z_{p0}^2$ prediction manifest. The smaller the sphere radius is (or the larger the z_{p0} value is), in terms of the

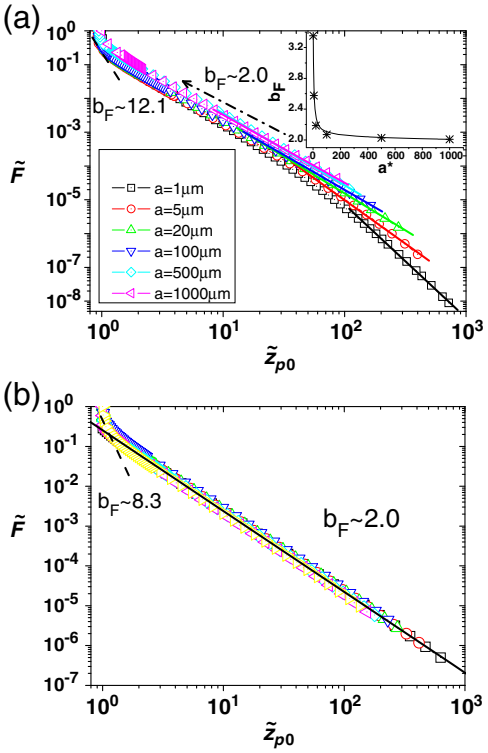

Fig. 12. (a) Scaled behavior of $\tilde{F}(0, \tilde{z}_{p0})$ for $z(0,z_{p0})$ data (with respect to varying the sphere radius) presented in Fig. 10(b) as functions of the scaled $\tilde{z}_{p0}$, the inset shows the dependence of b_F on the normalized sphere size (a^*, where $a^* \equiv a/a_0$ and $a_0 = 1$ μm) when the spherical solids are far from the limiting position. (b) Scaled behavior of $\tilde{F}(0, \tilde{z}_{p0})$ for $z(0,z_{p0})$ data (with respect to varying the Hamaker constant) presented in Fig. 11(b) as functions of the scaled $\tilde{z}_{p0}$.

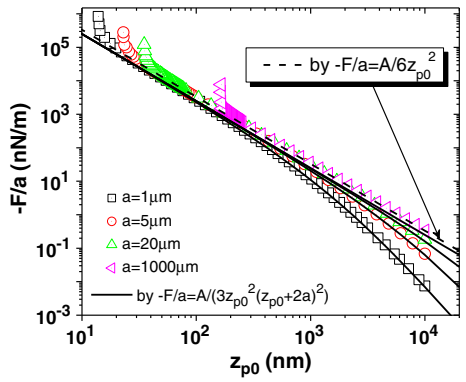

Fig. 13. Normalized force $(-F/a)$ versus z_{p0} curves of the attractive nonretarted vdW interaction between an infinite plane air–water interface and spherical solids of various radius. The symbol curves are obtained by replotting corresponding results of Fig. 10b after dividing the force data by the corresponding sphere radius. The solid curve is calculated from the expression[4,5,43,44], $F=-2Aa^3/(3z_{p0}^2(z_{p0}+2a)^2)$ with $A=2\times10^{-19}$ J; and the dashed one is from the well-known DA-based sphere-flat expression[4,5,43,44], $F=-Aa/6(z_{p0})^2$. It is known that $F=-2Aa^3/(3z_{p0}^2(z_{p0}+2a)^2)$ can be simplified to be $F=-Aa/6(z_{p0})^2$ through assuming z_{p0} is small compared to the radius a, which is the same as the base assumption of the Derjaguin approximation[3–6,39,43].

previous analysis [3,44] more obvious the invalidation of the Derjaguin approximation is, and more obvious the deviation from the $F/a=-A/6z_{p0}^2$ prediction appears.

From the above analysis it can be seen that, in contrast to the previous PS model that is available only for the macroscopic paraboloid solid, the SS theoretical model has the validity and advantage to provide a more accurate, and quantitative theoretical support to interpret the force-vs-distance (or the deformation-vs-distance) behaviors detected in the CP-AFM (or common AFM, or SFA) experiment involving the microscopic or submacroscopic probes. Corresponding necessary AFM experiments in our lab are to be performed in future.

4.4. Minimum allowed heights of the microscopic or submacroscopic spherical particle, and maximum induced deformation of fluid interface

The last problems we are to be concerned are how closely can a microscopic or submacroscopic solid approach an air–water surface without becoming wet, and how large the maximum vdW-induced deformation of the fluid interface. Similar issue for the macroscopic paraboloid shaped solid had been discussed on basis of the PS model system [24], but the previous PS-model prediction [24] is valid only in cases of the macroscopic paraboloid shaped solid when the DA approximation validates. It is necessary to perform a further investigation on this practical and fundamental problem on basis of the SS model system, aiming to give people a more quantitative and correct understanding of this problem involving note only the macroscopic solids but also the microscopic or submacroscopic ones.

As the previous studies [24], in this paper our focus is on the dependences of the critical limiting points, $z(0;z_{p0,\min})$, on the sphere radius (of $a\in[1500]\mu m$) and the Hamaker constant (of $A\in[2500]\times10^{-21}$ J), and on the comparison with the corresponding PS-model predictions in the range $\lambda\in[100,10,000]m^{-1}$, which were claimed previously [24,25] to be applicable in experiments quantifying the mesoscopic interaction between microscopic or submacroscopic solids and fluid interfaces. Thereinto, values of $z(0;z_{p0,\min})$ are determined in terms of the solvability limits [34,36–39] of the governing profile equation, viz. Eq. (15).

Fig. 14 respectively shows critical limiting values of z_{p0} and $z(0)$ as functions of the sphere radius (a) and the Hamaker constant (A) obtained on basis of the SS model. It is clear that, quite similar to the PS-model prediction shown as dashed and dashed dot curves in Fig. 14, as the size of the approaching sphere becomes larger or the

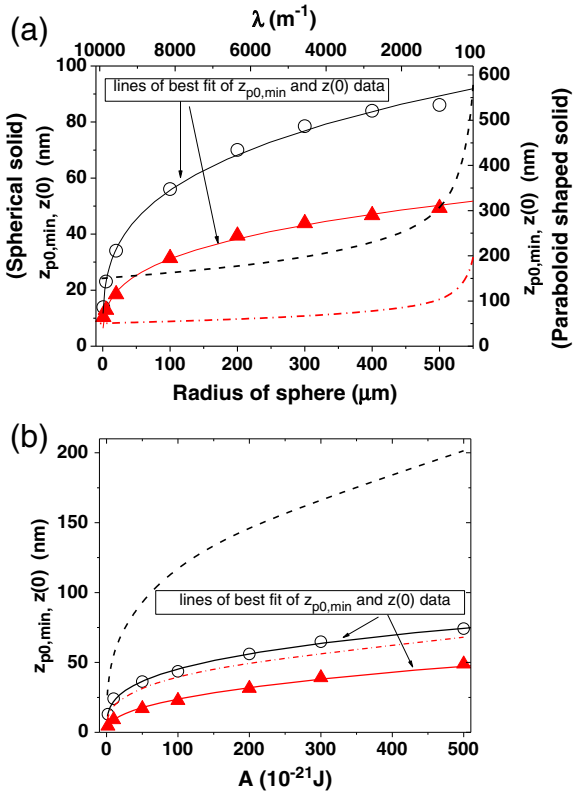

Fig. 14. Critical limiting heights (open squares) of an approaching spherical particle above a planar air–water surface as a function of the sphere radius (a) and the Hamaker constant (b). Solid triangles show the maximum heights of air–water interface. Solid curves are least squares fits to the numerical data of $z_{p0,\min}$ and $z(0)$ respectively. Dash and dash dot lines in (a) and (b) are the corresponding numerical results based on the PS model. Physical parameter values: $\Delta\rho=996.910$ kg/m^3, $\gamma=72$mN/m and fixed Hamaker constant $A=2.0\times10^{-19}$ J for (a); fixed radius parameter $a=100$ μm and fixed splay parameter $\lambda=10{,}000$ m^{-1}for (b).

vdW interaction strength increases, the limiting height of approach and the limiting maximum deformation of fluid interface, as well as the limiting separation between the sphere and fluid interface, gradually increase, due to the increase of the average surface pressure $P_z(r,z)$ strength on the fluid interface with increasing a or A (as shown in Fig. 8b and c).

Nevertheless, the limiting heights of the spheres of (1~1000) μm order and the corresponding maximum deformation of the air–water interface, predicted by the SS model system, are obviously smaller than the PS-model predictions in the range of $\lambda\in[100,10,000]m^{-1}$. The limiting value of $z(0)$ of the air–water interface induced by the sphere of $a=1$ μm, for instance (see Fig. 14a), is predicted by the SS model to be approximate 10.0 nm, whereas the limiting value of $z(0)$ induced by the paraboloid solid with $\lambda=10{,}000$ m^{-1} is predicted by the PS model to be approximate 60.0 nm, in particular the one for $\lambda=100$ m^{-1} is predicted to be up to 200.0 nm. By comparing with the practical expectations [2,4,5], these PS-model predictions seems grossly overestimated and unreasonably large. In terms of the previous analysis, we can know that, it mostly results from the gross overestimation of the vdW interaction by the Derjaguin approximation technique in the PS model for the cases of the microscopic or submacroscopic solids; whereas the SS model conquers such restriction and can thus provide a more accurate, quantitative and more reasonable prediction to the critical limiting behavior of a microscopic or submacroscopic solid approaching toward the air–water interface.

In addition, as in the previous studies [24], from the SS-model predicted numerical data in Fig. 14 and using the nonlinear

function ($f(a;A)=a^{\alpha}A^{\beta}$) to fit these numerical data, we can obtain a least-squares fits of the form

$$z_{p0,\,min}\,(a=100\mu m;A)\approx\left(10^{-4}\right)^{\alpha_1}A^{\beta_1}(\mathrm{m}) \tag{19a}$$

$$z_{p0,\,min}\left(a;A=2\times10^{-19}J\right)\approx a^{\alpha_2}\left(2\times10^{-19}\right)^{\beta_2}(\mathrm{m}) \tag{19b}$$

with exponent values $\alpha_1=0.3639$, $\beta_1=0.3099$ and $\alpha_2=0.2950$, $\beta_2=0.3248$. From Eq. (19a) and (19b) and in light of the method to deducing the closed-form analytic expression of $z_{p0,\min}$ in the previous refs [24,25,27], it thus can be possible to assume that the parameter dependence of $z_{p0,\min}$ for the approaching spherical particle toward the air–water interface be of the form

$$z_{p0,\,min}(a;A)\approx a^{\alpha(a,A)}A^{\beta(a,A)}, \tag{20a}$$

Thus, given the maximum height of an isolated sessile drop above a fixed reference level in a typical CM-AFM experiment, Eq. (20a) can be used to more quantitatively and correctly determine the minimum possible substrate-colloidal particle separation. Likewise, the maximum value of the peak in the air–water profile, $z(0)$, also naturally follows the trend in the $z_{p0,\min}$ values, it thus could also give

$$z(0;a;A)\approx a^{\tau(a,A)}A^{\mu(a,A)}, \tag{20b}$$

where the exponents α, β, τ and μ in Eqs. (20a) and (20b) are the functions of the radius of the sphere (a) and the vdW interaction strength (A).

Consequently, how closely can a microscopic or submacroscopic solid approach an air–water surface without becoming wet, and how large the maximum induced deformation of the fluid interface? Comparing with the previous forms of $z_{p0,\min}=10^{\alpha(\lambda)}A^{\beta(\lambda)}$ and $z(0)_{\max}=10^{\tau(\lambda)}A^{\mu(\lambda)}$ deduced on basis of the PS model system, Eqs. (20a) and (20b) provide a more correct and quantitative answer to this question. Note that exact functions of the exponents (e.g. α, β, τ and μ) in Eqs. (20a) and (20b) can be determined through respectively varying A and a, in this paper we would not employ larger space to further reiterate this simple but tortuous fitting work, for details see the previous Refs[25,27].

5. Summary and final remarks

In this paper we have derived an exact and analytic expression Eq. (12) for the attractive nonretarded vdW attraction energy between a spherical particle and a planar surface interface of unit area by pairwise integrating the interaction of the form $w(l)=-C/l^n$ of all the atoms in the sphere and the unit area planar surface. Through employing this Eq. (12) technique and modeling the solid as a spherical particle, an improved spherical solid model system following the previous paraboloid shaped solid model is thus developed to more accurately and quantitatively study the vdW-induced deformation of an infinite plane fluid interface interacting with an approaching microscopic or submacroscopic spherical solid.

The major advantage of this improved theory is that it provides a straightforward and available technique for exactly scaling the vdW surface energy density of the deformed fluid interface and the corresponding total vdW interaction energy, thus successfully ruling out the limitations of the previous PS model and other corresponding theoretical work based on the Derjaguin approximation for cases of the microscopic or submacroscopic solids. The validity and advantage of the SS model is evidently and rigorously demonstrated through applying the improved SS model to successfully numerically-address some practical and fundamental problems in this field (that are still ambiguous as yet or poor predicted by the PS model) and comparing with the corresponding PS-model predicted numerical results and the predictions by the Hamaker's sphere-flat expression and the general DA-based technique (viz. $F/a=-A/6z_{p0}^2$).

We believe that the capability of the SS model to provide exact results for the interaction energy between a deformed fluid interface and a spherical solid might be useful in accurate and quantitative interpretation of AFM (in particular the CP-AFM) data, since the model of the fluid interface interacting with the sphere well emulates the practical situation encountered in AFM. The experiment by AFM with the colloidal probe to experimentally validate the theoretical prediction concerned in this paper is being performed in our laboratory, we hope to elaborate on it in a future publication.

Acknowledgement

This work was supported in part by China Postdoctoral Science Foundation (Grant No. 20090460810) and by the Research Fund for the Postdoctoral program of Sun Yat-sen University of China (Grant No. 30000-4204714).

References

[1] J. Leja, Surface Chemistry of Froth Flotation, Plenum, New York, 1982.
[2] W.A. Ducker, Z.G. Xu, J.N. Israelachvili, Langmuir 10 (1994) 3279.
[3] J.N. Israelachvili, Intermolecular and Surface Forces, 2nd ed, Academic Press, New York, 1992.
[4] B. Cappella, G. Dietler, Surf. Sci. Rep. 34 (1999) 1.
[5] H.–J. Butt, B. Cappela, M. Kappl, Surf. Sci. Rep. 59 (2005) 1.
[6] J.N. Israelachvili, D. Tabor, Proc. R. Soc. Lond. A331 (1972) 19.
[7] J.N. Israelachvili, G.E. Adams, J. Chem. Soc. Faraday Trans. I 74 (1978) 975.
[8] P.M. Claesson, et al., Adv. Colloid Interface Sci. 67 (1996) 119.
[9] J.C. Froberg, O.J. Rojas, P.M. Claesson, Int. J. Miner. Process. 56 (1999) 1.
[10] G. Binnig, C.F. Quate, C. Gerber, Phys. Rev. Lett. 56 (1986) 930.
[11] F.J. Giessibl, Rev. Mod. Phys. 75 (2003) 945.
[12] H.–J. Butt, M. Jaschke, W. Ducker, Bioelectrochem. Bioenerg. 38 (1995) 191.
[13] M. Kappl, H.–J. Butt, Part. Part. Syst. Char. 19 (2002) 129.
[14] R.R. Dagastine, et al., Science 313 (2006) 210.
[15] F.R. Zypman, J. Phys. Condens. Matter 18 (2006) 2795.
[16] G.B. Webber, et al., Soft Matter 4 (2008) 1270.
[17] N.H. Chen, et al., Phys. Rev. Lett. 92 (2004) 024501.
[18] M.L. Forcada, M.M. Jakas, A. Gras-Marti, J. Chem. Phys. 95 (1991) 706.
[19] M.L. Forcada, J. Chem. Phys. 98 (1993) 638.
[20] M. Preuss, H.J. Butt, Langmuir 14 (1998) 3164.
[21] M. Preuss, H.–J. Butt, Int. J. Miner. Process. 56 (1999) 99.
[22] D.Y.C. Chan, R.R. Dagastine, L.R. White, J. Colloid Interface Sci. 236 (2001) 141.
[23] R.R. Dagastine, L.R. White, J. Colloid Interface Sci. 247 (2002) 310.
[24] F.P.A. Cortat, S.J. Miklavcic, Phys. Rev. E 68 (2003) 052601.
[25] F.P.A. Cortat, S.J. Miklavcic, Langmuir 20 (2004) 3208.
[26] S.J. Miklavcic, L.R. White, Langmuir 22 (2006) 6961.
[27] Y.Z. Wang, D. Wu, X.M. Xiong, J.X. Zhang, Langmuir 23 (2007) 12119.
[28] D. Wu, Y.Z. Wang, J.X. Zhang, Chin. Phys. Lett. 24 (2007) 2914.
[29] S.J. Miklavcic, R.G. Horn, D.J. Bachmann, J. Phys. Chem. 99 (1995) 16357.
[30] B.A. Todd, S.J. Eppell, Langmuir 20 (2004) 4892.
[31] D.J. Bachmann, S.J. Miklavcic, Langmuir 12 (1996) 4197.
[32] R.G. Horn, et al., J. Phys. Condens. Matter 8 (1996) 9483.
[33] S.J. Miklavcic, P. Attard, J. Phys. A: Math. Gen. 34 (2001) 7849.
[34] D.E. Aston, J.C. Berg, J. Colloid Interface Sci. 235 (2001) 162.
[35] S.J. Miklavcic, P. Attard, J. Phys. A: Math. Gen. 35 (2003) 4335.
[36] S.J. Miklavcic, J. Phys. A: Math. Gen. 36 (2003) 8829.
[37] D.C. Bardos, Surf. Sci. 517 (2002) 157.
[38] S. Bhattacharjec, A. Sharma, Langmuir 12 (1996) 5498.
[39] S. Bhattacharjec, M.J. Elimelech, Colloid Interface Sci. 193 (1997) 273.
[40] S.I. Zanette, et al., Surf. Sci. 453 (2000) 75.
[41] A microscopic or submacroscopic solid is often defined to be have the size within 1000 nm, e.g. the common AFM tip with curvature radius of 10 100 nm and the CP-AFM colloid probe in use in experiments having the radius of μm order [2–5]. From Eqs. (11) and (12) in Ref[24] and data of Table 2 in Ref[25], the limiting separation range for a microscopic or submacroscopic paraboloid shaped solid is approximate 400 100 nm. Moreover, during calculating the vdW interaction in the PS model, the involved separations between the microscopic (or submacroscopic) paraboloid shaped solid and the fluid interface are often much larger than its limiting one.
[42] H.C. Hamaker, Phys. Amsterdam 4 (1937) 1058.
[43] S. Basu, M.M. Sharma, J. Colloid Interface Sci. 181 (1996) 443.
[44] C. Argento, R.H. French, J. Appl. Phys. 80 (1996) 6081.
[45] R. Courant, D. Hilbert, R. Courant, D. Hilbert, Methods of Mathematical Physics, vol. 1, Wiley, New York, 1965.